

# Tricyclic Isatin Derivatives as Anti-Inflammatory Compounds with High Kinase Binding Affinity

Alexander V. Uvarov, Igor A. Schepetkin, Mark T. Quinn  
and Andrei I. Khlebnikov

Uvarov, A.V.; Schepetkin, I.A.; Quinn, M.T.; Khlebnikov, A.I. Tricyclic Isatin Derivatives as Anti-Inflammatory Compounds with High Kinase Binding Affinity. *Molecules* 2025, 30, 2914. <https://doi.org/10.3390/molecules30142914>

**Accessibility Disclaimer:**

For a more accessible version of this document, please submit an accessibility request form through the Montana State University Library website.

## Article

# Tricyclic Isatin Derivatives as Anti-Inflammatory Compounds with High Kinase Binding Affinity

Alexander V. Uvarov <sup>1</sup>, Igor A. Schepetkin <sup>2,\*</sup>, Mark T. Quinn <sup>2</sup>  and Andrei I. Khlebnikov <sup>1,\*</sup> <sup>1</sup> Kizhner Research Center, Tomsk Polytechnic University, Tomsk 634050, Russia; avu12@tpu.ru<sup>2</sup> Department of Microbiology and Cell Biology, Montana State University, Bozeman, MT 59717, USA; mquinn@montana.edu

\* Correspondence: igor@montana.edu (I.A.S.); aikhl@chem.org.ru (A.I.K.)

## Abstract

Oximes have been reported to exhibit useful pharmaceutical properties, including compounds with anticancer, anti-arthritis, antibacterial, and neuroprotective activities. Many oximes are kinase inhibitors and have been shown to inhibit various kinases. Herein, a panel of oxime derivatives of tricyclic isatins was synthesized and evaluated for inhibition of cellular inflammatory responses and binding affinity to several kinases. Compounds **5a** and **5d** (a.k.a. NS-102), which have an unsubstituted oxime group, inhibited lipopolysaccharide (LPS)-induced nuclear factor- $\kappa$ B/activating protein 1 (NF- $\kappa$ B/AP-1) transcriptional activity in human THP-1Blue monocytic cells and interleukin-6 (IL-6) production in human MonoMac-6 monocytic cells, with IC<sub>50</sub> values in the micromolar range. These compounds also inhibited LPS-induced production of several other proinflammatory cytokines, including IL-1 $\alpha$ , IL-1 $\beta$ , monocyte chemoattractant protein-1 (MCP-1), and tumor necrosis factor (TNF) in MonoMac-6 cells. Compounds **5a** and **5d** exhibited nanomolar/submicromolar binding affinity toward several kinase targets. The most potent inhibitor, **5d** (3-(hydroxyimino)-5-nitro-1,3,6,7,8,9-hexahydro-2H-benzo[g]indol-2-one), demonstrated high binding affinity for 12 kinases, including DYRK1A, DYRK1B, PIM1, Haspin, HIPK1-3, IRAK1, NEK10, and DAPK1-3. Molecular modeling suggested modes of binding interaction of selected compounds in the DYRK1A and PIM1 catalytic sites that agreed with the experimental binding data. Our results demonstrate that tricyclic isatin oximes could be potential candidates for developing anti-inflammatory drugs with neuroprotective effects for treating neurodegenerative diseases.

**Keywords:** dual-specificity tyrosine phosphorylation-regulated kinase 1 A (DYRK1A); proviral insertion site in Moloney murine leukemia virus (PIM); isatin; aryl oxime; NS-102; anti-inflammatory; cytokine



Academic Editors: Maria Maddalena Cavalluzzi and Giovanni Lentini

Received: 11 June 2025

Revised: 30 June 2025

Accepted: 8 July 2025

Published: 10 July 2025

**Citation:** Uvarov, A.V.; Schepetkin, I.A.; Quinn, M.T.; Khlebnikov, A.I.Tricyclic Isatin Derivatives as Anti-Inflammatory Compounds with High Kinase Binding Affinity. *Molecules* **2025**, *30*, 2914. <https://doi.org/10.3390/molecules30142914>**Copyright:** © 2025 by the authors. Licensee MDPI, Basel, Switzerland. This article is an open access article distributed under the terms and conditions of the Creative Commons Attribution (CC BY) license (<https://creativecommons.org/licenses/by/4.0/>).

## 1. Introduction

Protein kinases play a central role in cellular signaling and regulation, serving as key modulators of various physiological processes. Dual-specificity tyrosine phosphorylation-regulated kinase 1 A (DYRK1A), proviral insertion site in Moloney murine leukemia virus (PIM), and Haspin (haploid germ cell-specific nuclear protein kinase) have emerged as significant kinase targets for the treatment of cancer, neurodegenerative diseases, and inflammatory diseases at the clinical and preclinical levels [1–6]. The known substrates of DYRK1A include proteins involved in transcription, cell cycle control, DNA repair, and other processes [7]. Overexpression of DYRK1A has also been proposed to be a

significant contributor to the underlying neurodevelopmental abnormalities associated with Down syndrome [8]. Likewise, elevated DYRK1A immunoreactivity has been linked to neurofibrillary tangle pathology in Alzheimer's disease (AD) [9]. Additionally, DYRK1A is involved in the phosphorylation of tau protein on sites that are hyperphosphorylated during the course of tau pathology in AD [1].

PIM proteins are evolutionarily conserved serine/threonine kinases consisting of PIM1–3. PIM1 is a constitutively active, highly conserved, pleiotropic, and multifunctional kinase that regulates many cellular functions, such as proliferation, apoptosis, and cell functional activity [2,3]. Recently, PIM1 inhibitors have been developed as potential therapeutics to reduce neuropathology in AD [10]. Haspin is highly upregulated in a variety of cancers, such as bladder cancer, colorectal, ovarian cancer, breast cancer, Burkitt's lymphoma, and chronic lymphocytic leukemias [4–6]. Moreover, Haspin was expressed in the hippocampus and phosphorylated tau protein and may be one of the target molecules for the repression of tau phosphorylation in the treatment of AD [11].

Kinase inhibitors target several molecular pathways involved in differentiation and cellular growth and have been used in the treatment of cancer and inflammatory diseases [12]. For example, several pharmacological small-molecule inhibitors of PIM1 have been preclinically and clinically evaluated and were found to exhibit therapeutic potential [13,14]. DYRK1A inhibitors have a high therapeutic potential for pharmacological intervention in diabetes mellitus, neurodegenerative diseases, and cancer [15,16]. Although inhibitors of Haspin have not yet been widely explored, several scaffolds (e.g., derivatives of  $\beta$ -carboline, acridine, and 5-iodotubercidin) have emerged as agents with promising therapeutic potential [17].

Drug repositioning is the process of finding new clinical applications for existing drugs [18]. Off-target effects are typically unwanted and may be harmful, but in some cases, they have proven to be beneficial, resulting in new and unexpected uses for drugs [19]. Currently, heterocyclic compounds containing an oxime group in their structure are of considerable interest. For example, we found that 11*H*-indeno[1,2-*b*]quinoxalin-11-one oxime (compound IQ-1) and tryptanthrin-6-oxime derivatives inhibited enzymes of the c-Jun *N*-terminal kinase (JNK) family, which are regulators of inflammatory processes and cell proliferation [20–23]. Other aryl oximes with an isatin moiety have also been reported to have anticancer and anti-inflammatory potential [24,25]. It should be noted that the indole structure of isatin is a fundamental fragment of many known biologically active compounds of natural and synthetic origin [26]. Thus, it is reasonable that known aryl oximes could be used in screening of kinase targets to identify novel therapeutics. Additionally, multitargeting compounds to target multiple protein kinases as well as some receptors (i.e., *N*-methyl-D-aspartate (NMDA) receptors) involved in other processes related to AD could be useful for the development of potential therapeutics to treat neurodegenerative diseases [27,28].

There are several commercially available aryl oximes with known pharmacological effects. For example, it has been shown that domoic acid toxicity is reduced by treatment with the selective GluR6 antagonist NS-102 [29,30]. NS-102 was also used in other animal models as a GluK2 antagonist [31–33]. Thus, we pursued studies to provide further insight into the specificity of various previously described aryl oximes and identify novel and potential kinase inhibitors with anti-inflammatory activity. To accomplish this goal, NS-102 (3-(hydroxyimino)-5-nitro-1,3,6,7,8,9-hexahydro-2*H*-benzo[*g*]indol-2-one, designated in this report as compound **5d**) was screened across a panel of over 423 human kinases. Furthermore, several additional analogues of NS-102 (compounds **5a–c,e,f**) were synthesized and tested for biological activity *in vitro*. Importantly, molecular modeling suggested modes of binding interaction of compounds **5a** and **5d** in DYRK1A and PIM1 that agreed with the

experimental binding data. We also evaluated activity of the structurally related oxime NS-383 (8-ethyl-6,7,8,9-tetrahydro-5-phenyl-1*H*-pyrrolo[3,2-*h*]isoquinolin-2,3-dione-3-oxime), which is an inhibitor of acid-sensing ion channels (ASICs) [18,34]. ASICs have also been linked to several neurological disorders, such as AD and Parkinson's disease [35].

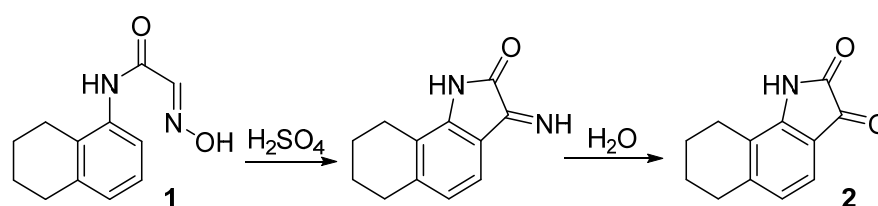
## 2. Results and Discussion

### 2.1. Chemical Synthesis

While certain tricyclic isatin analogues, including NS-102 and its precursors, have been previously reported [36], synthesis of these compounds in high purity has remained challenging due to the severe conditions required for their formation. In this study, we present optimized synthetic conditions for NS-102 (indicated here as **5d**) and its key precursors, 6,7,8,9-tetrahydro-1*H*-benzo[*g*]indol-2,3-dione and 5-nitro-6,7,8,9-tetrahydro-1*H*-benzo[*g*]indol-2,3-dione. Our approach aimed to achieve an optimal balance between preparative yield and purity of these compounds.

#### 2.1.1. Synthesis of NS-102 Precursors

One of the methods for isatin ring formation utilizes Sandmeyer isatin synthesis [37], which uses unsubstituted oximes based on acetanilides. Sandmeyer intramolecular cyclization occurs in strongly acidic media and involves the *ortho*-carbon atom, resulting in formation of a fused pyrrole ring containing carbonyl and imino groups in positions 2 and 3, respectively. The imino group of this intermediate can be readily hydrolyzed to form the second carbonyl group of the isatin. The Sandmeyer cyclization of 2-(hydroxyimino)-*N*-(5,6,7,8-tetrahydronaphthalen-1-yl)acetamide (**1**) to the NS-102 precursor 6,7,8,9-tetrahydro-1*H*-benzo[*g*]indol-2,3-dione (**2**) is represented in Scheme 1.



**Scheme 1.** The synthesis of 6,7,8,9-tetrahydro-1*H*-benzo[*g*]indol-2,3-dione (**2**).

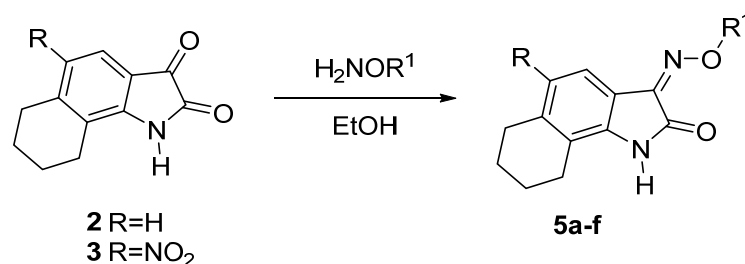
Despite the simplicity of the transformations during the synthesis of isatins according to Sandmeyer, some experimental difficulties arise due to structural features of acetanilides and tarring of the reaction mass in highly acidic media. The yield of isatins depends on the cyclization temperature (20–100 °C) and the concentration of sulfuric acid. In most cases, 98% sulfuric acid is used. Lower concentrations of H<sub>2</sub>SO<sub>4</sub> can be used for the cyclization of easily sulfonated isonitrosoacetanilides; however, the resulting isatin may be contaminated with isatin-3-oxime [38]. Instead of H<sub>2</sub>SO<sub>4</sub>, some authors [39] have proposed the use of polyphosphoric acid (PPA) as a cyclizing agent. Nevertheless, in comparison with sulfuric acid, this method has not found wide application due to the possible formation of by-products, such as *N*-phenyloxamide derivatives [38].

Varying the concentration of sulfuric acid and temperature, we optimized conditions of the Sandmeyer synthesis to obtain the tricyclic isatin analogue **2** in good yields. The results showed that success of the cyclization depended strongly on the H<sub>2</sub>SO<sub>4</sub> concentration. It was found that maintaining the temperature at 50 °C and using 75% solution of H<sub>2</sub>SO<sub>4</sub> gave the highest yield of compound **2** (90%). In addition, the maximum level of acetanilide **1** conversion (98%) was achieved under these conditions. Our protocol minimized the formation of tarry by-products and led to compound **2** in sufficient purity for further



**Table 2.** The oximation of isatin derivatives.

Compd.	R	R <sup>1</sup>	Yield (%)
5a	H	H	96
5b	H	Me	93
5c	H	Et	89
5d	NO <sub>2</sub>	H	95
5e	NO <sub>2</sub>	Me	90
5f	NO <sub>2</sub>	Et	90

**Scheme 3.** Oximation of the tricyclic isatins.

## 2.2. Biological Activity

### 2.2.1. Anti-Inflammatory Activity (In Vitro)

Prior to evaluation of the compounds in cell-based assays, we measured their cytotoxicity in human monocytic THP-1Blue and MonoMac-6 cells during a 24 h incubation. NS-383 was cytotoxic in both cell lines. Thus, this compound was excluded from subsequent testing in cell cultures (Table 3).

**Table 3.** Analysis of compounds effects on LPS-induced NF- $\kappa$ B/AP-1 transcriptional activity, interleukin 6 (IL-6) production, and cytotoxicity.

Compd.	AP Production (THP-1 Cells)	IL-6 Production (MonoMac-6 Cells)	Cytotoxicity (THP-1 Cells)	Cytotoxicity (MonoMac-6 Cells)
	IC <sub>50</sub> ( $\mu$ M)			
5a	6.0 $\pm$ 1.3	48.3 $\pm$ 4.4	N.T.	N.T.
5b	N.A.	N.A.	N.T.	N.T.
5c	N.A.	N.A.	N.T.	N.T.
5d	5.5 $\pm$ 1.4	12.6 $\pm$ 3.2	N.T.	N.T.
5e	N.A.	N.A.	N.T.	N.T.
5f	N.A.	N.A.	N.T.	N.T.
NS-383	n.d.	n.d.	19.2 $\pm$ 2.1	21.2 $\pm$ 2.4

N.T.: no cytotoxicity was found at concentrations up to 50  $\mu$ M. AP: alkaline phosphatase. N.A.: compound was not active at the highest tested concentration (50  $\mu$ M); n.d.: no data (activity of the compound was not evaluated because of its cytotoxicity).

Compounds lacking cytotoxic activity were further evaluated for anti-inflammatory activity. Anti-inflammatory activity was assessed by determining the compound's capacity to inhibit lipopolysaccharide (LPS)-induced NF- $\kappa$ B/AP-1 activity in THP-1Blue monocytic cells, as this pathway is essential in phagocyte inflammatory responses [42]. We also evaluated the effect of compounds on IL-6 production by MonoMac-6 monocytic cells. Compounds **5a** and **5d** were relatively potent inhibitors of NF- $\kappa$ B/AP-1 reporter activity in THP-1Blue cells, with IC<sub>50</sub> values < 6.1  $\mu$ M (Table 3). As an example, the dose-dependent inhibition of LPS-induced NF- $\kappa$ B/AP-1 activity by compounds **5a** and **5d** is shown in Figure 1A. Compounds **5a** and **5d** also inhibited IL-6 production in MonoMac-6 cells

(Table 3). As an example, the dose-dependent inhibition of LPS-induced IL-6 production is shown in Figure 1B. These results indicate that alkylation of the oxime group (compounds 5b, 5c, 5e, and 5f) led to the loss of biological activity, indicating that the unsubstituted oxime function =N-OH is important for effective kinase binding.

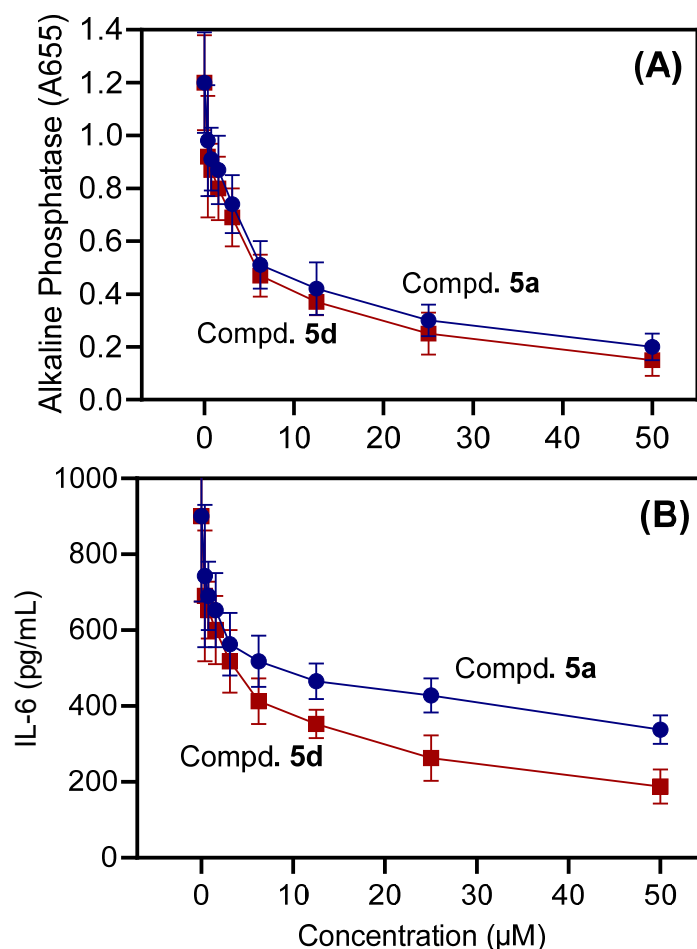


**Figure 1.** Analysis of the capacity of 5a and 5d to inhibit NF-κB/AP-1 activity and IL-6 production. (A): After THP-1Blue monocytic cells were treated with test compounds or control DMSO for 30 min, 250 ng/mL LPS or buffer was added, and the cells were incubated for 24 h. We analyzed NF-κB/AP-1 activity by measuring secreted alkaline phosphatase activity in the cell supernatants (absorbance at 655 nm). (B): After MonoMac-6 monocytic cells were treated with test compounds or control DMSO for 30 min, 250 ng/mL LPS or buffer was added, and the cells were incubated for 24 h. We determined IL-6 levels in the supernatants using ELISA, as described. The data in both panels represent the mean ± S.D. of triplicate samples from one experiment, which is from three independent experiments.

The effect of compounds 5a, 5b, 5d, and 5e on the production of an array of seven different proinflammatory cytokines and chemokines was also investigated using a Multiplex human cytokine ELISA kit. Compound 5d, at a concentration of 10 μM, inhibited the secretion of IL-1α, IL-1β, IL-6, tumor necrosis factor (TNF), and monocyte chemoattractant protein-1 (MCP-1) in LPS-stimulated MonoMac-6 cells compared with dimethyl sulfoxide (DMSO)-treated control cells. The effect on granulocyte-macrophage colony-stimulating factor (GM-CSF) and interferon-γ (IFN-γ) production was inconclusive because of the low production of these cytokines after LPS treatment of MonoMac-6 cells (Figure 2). Compound 5a was less effective in the inhibition of cytokine production, and compounds 5b and 5e were ineffective. These data further demonstrate the anti-inflammatory activity of 5a and 5d.

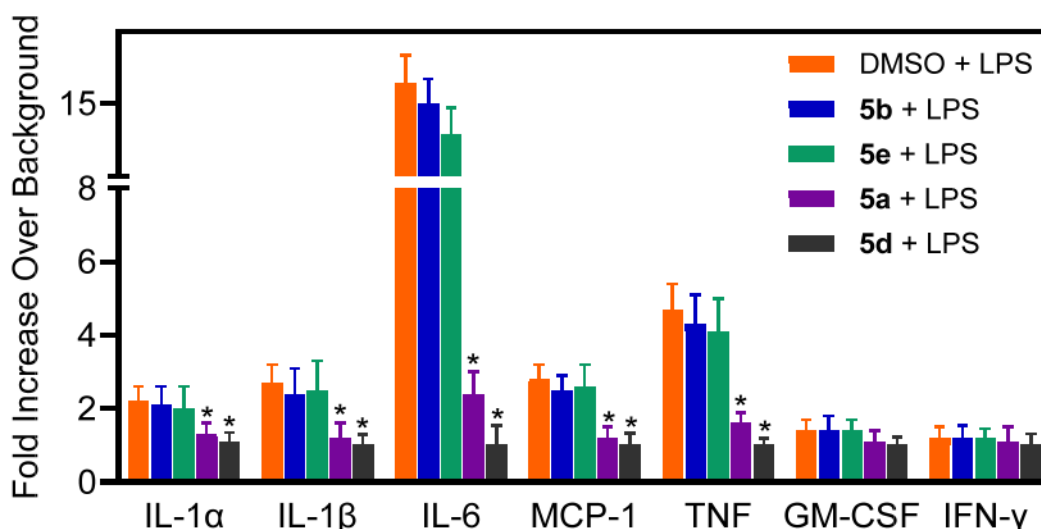


Figure 2. Effect of compounds 5a, 5b, 5d, and 5e on proinflammatory cytokine production in MonoMac-6 cells. Human MonoMac-6 monocytic cells were pretreated with 10  $\mu$ M of the tested compounds or DMSO for 30 min, followed by addition of 250 ng/mL LPS or buffer for 24 h. Production of cytokines in the supernatants was evaluated using a Multiplex human cytokine ELISA kit. The relative level of cytokine production is shown as the fold increase over background (i.e., 1% DMSO control, without LPS). The data are presented as the mean  $\pm$  S.D. of triplicate samples from one experiment that is representative of two independent experiments. \*  $p < 0.05$  in comparison with the control group (DMSO + LPS).

### 2.2.2. Identification of Potential Kinase Targets

Protein kinases play critical roles in the regulation of NF- $\kappa$ B/AP-1 transcriptional activity. Thus, compound 5d, which demonstrated potent inhibitory activity in all cell-based assays (Table 3), was profiled in a competition binding assay for its ability to compete with an active site-directed ligand for 423 different kinases (including mutated forms), representing all known kinase families (DiscoverX KINOMEScan). Compound 5d was screened at 10  $\mu$ M, which was a concentration that effectively inhibited biological activity (see Figure 1). The kinases for which >96% inhibition of ligand binding and kinase activity was observed were designated as “kinase targets of the compound.” Twelve such kinase targets were identified, including DAPK1-3, DYRK1A, DYRK1B, Haspin, HIPK1-3, IRAK1, NEK10, and PIM1. Results for the percentage inhibition of binding to the active site-directed ligand for all of the 423 kinases after treatment with 10  $\mu$ M 5d are shown in Supplementary Materials Table S2, and data for the 12 selected kinase targets are shown in Table 4. The selectivity score,  $S(10)$ , based on >90% inhibition of ligand binding at a single 10  $\mu$ M screen concentration, was calculated by dividing the “kinase targets of the compound” with the “total number of nonmutated kinases” in the panel [43]. The published kinase profile of SP600125, a well-known c-Jun N-terminal kinase (JNK) inhibitor [44], was used to determine its  $S(10)$  value. We found that the  $S(10)$  for 5d was much lower ( $0.073 = 31/423$ ) compared with the  $S(10)$  for SP600125 ( $0.328 = 39/119$ ), indicating much higher target kinase selectivity for 5d. Three compounds (5a, 5d, and NS-383) were submitted for determination of their binding affinities ( $K_d$ ) to the target kinases that exhibited the highest binding activity for compound 5d in the primary kinase profiling. As shown in Table 4, compound 5d had  $K_d$  values in the nanomolar range for all of tested kinase targets. Compound 5a was less potent in the binding affinity, and NS-383 had low binding affinity for only PIM1.

**Table 4.** Inhibition of ligand binding by **5d** and  $K_d$  values for compounds **5d**, **5a**, and NS-383 against the twelve selected kinase targets.

Kinase Target	Inhibition (%) of Ligand Binding by <b>5d</b> (10 $\mu$ M)	Compd. <b>5d</b>	Compd. <b>5a</b>	NS-383
		$K_d$ ( $\mu$ M)		
DAPK1	96.3	$0.29 \pm 0.02$	$13.5 \pm 0.7$	N.B.
DAPK2	98.9	$0.20 \pm 0.042$	$7.7 \pm 1.1$	N.B.
DAPK3	98.5	$0.59 \pm 0.028$	$20.5 \pm 3.5$	N.B.
DYRK1A	98.8	$0.435 \pm 0.078$	$0.85 \pm 0.12$	N.B.
DYRK1B	96.4	$0.47 \pm 0.02$	N.B.	N.B.
Haspin	99.45	$0.165 \pm 0.021$	$0.61 \pm 0.08$	N.B.
HIPK1	98.5	$0.52 \pm 0.113$	$1.1 \pm 0.07$	N.B.
HIPK2	99.7	$0.295 \pm 0.092$	$0.73 \pm 0.64$	N.B.
HIPK3	100	$0.135 \pm 0.07$	$1.3 \pm 0.3$	N.B.
IRAK1	99.2	$0.67 \pm 0.113$	N.B.	N.B.
NEK10	100	$0.66 \pm 0.071$	$3.2 \pm 1.0$	N.B.
PIM1	98.2	$0.122 \pm 0.054$	$1.8 \pm 0.1$	$14.0 \pm 0.7$

N.B.: no binding was found at concentrations up to 30  $\mu$ M.

Previously, we reported that aryl oximes with tryptanthrin and related scaffolds have a high binding affinity for JNK1-3 [20–22]. The isatin-type tricyclic oximes studied here exhibited relatively low binding affinity for JNK1-3 (52–76% at 10  $\mu$ M concentration; Supplementary Materials Table S2). Although **5d** was inactive toward MKK7, this compound demonstrated a high binding activity (95.8% inhibition of the ligand binding) for mitogen-activated protein kinase 19 (MAP3K19), a kinase that directly activates the ERK and JNK cascades [45]. Thus, compound **5d** might be able to affect the JNK signaling pathway, although further studies are needed to assess this possibility.

### 2.3. Molecular Docking

We performed molecular modeling of the potential interaction of compounds **5a** and **5d** with DYRK1A, as our kinase screening indicated high affinity of these compounds for DYRK1A. Using the known structure of DYRK1A (PDB code 3ANQ) [46], we found the best docking pose of **5d** presented in Figure 3A. Molecule **5d** was strongly anchored in the DYRK1A binding site by hydrogen bonding to Asp307 and Lys188, with participation of the oxime OH group and amide oxygen atoms. Analogously, compound **5a** formed H-bonds with Lys188, Glu203, and Asp307 of DYRK1A (Figure 3B, Table 5). Note that the amino acid residues in closest proximity to **5a** and **5d** were also located in the vicinity of co-crystallized DYRK1A/B inhibitor INDY [47]. The orientations of compounds **5a** and **5d** within the binding site are very similar, with the oxime and C=O groups directed towards Glu203 and Asp307. However, molecule **5a** is flipped with respect to **5d**, possibly because of steric bulkiness and polarity of the nitro group. The interface scores obtained for both isatin analogues with the ROSIE ligand docking protocol are nearly 14 units, with a slightly higher value for the nitro-derivative **5d**. The inactive ethyl-substituted oximes **5f** and NS-383, which was docked into DYRK1A for comparative purposes, had noticeably lower interface scores (Table 5). Although compound NS-383 is anchored by hydrogen bonding interactions within the binding sites of DYRK1A and PIM1 (Table 5), the presence of bulky phenyl group and ethyl substituent in the ligand may hinder its effective binding to these kinases.

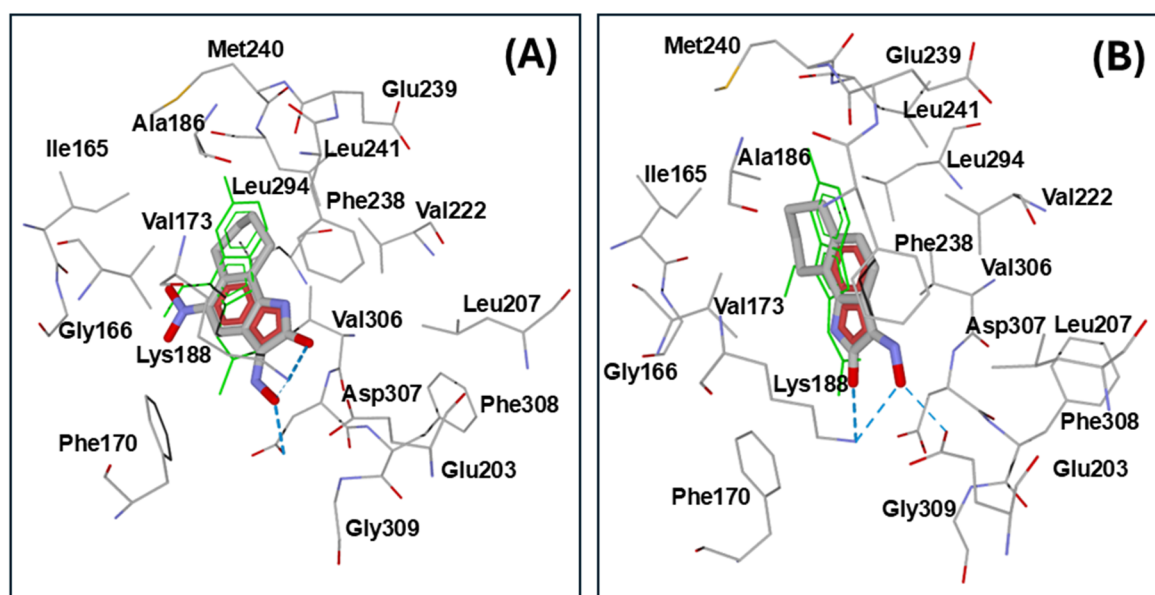


**Figure 3.** Docking poses of compounds **5d** (A) and **5a** (B) in DYRK1A binding site (PDB code 3ANQ). The co-crystallized ligand INDY [(1Z)-1-(3-ethyl-5-hydroxy-1,3-benzothiazol-2(3H)-ylidene)propan-2-one] is represented by thin green sticks. Residues within 4 Å from each pose are visible.

**Table 5.** The pose characteristics obtained for the docking of compounds **5d**, **5a**, and **5f** into kinase targets DYRK1A and PIM1.

Kinase (PDB Code)	Compd.	Interface Score *	Hydrogen Bonds **
DYRK1A (3ANQ)	<b>5d</b>	−14.11	Lys188 (carbonyl oxygen, oxime oxygen-weak), Asp307 (oxime OH)
	<b>5a</b>	−13.97	Lys188 (carbonyl oxygen, oxime oxygen), Glu203 (oxime OH), Asp307 (oxime nitrogen-weak)
	<b>5f</b>	−13.50	Lys188 (NO <sub>2</sub> oxygen), Asp307 (NO <sub>2</sub> oxygen)
	NS-383	−13.19	Lys188 (oxime nitrogen), Asp307 (oxime OH), Gly309 (oxime OH-weak)
PIM1 (2OBJ)	<b>5d</b>	−12.74	Glu121 (oxime OH), Asp186 (NO <sub>2</sub> oxygen), Lys67 (NO <sub>2</sub> oxygen)
	<b>5a</b>	−12.24	Arg122 (oxime nitrogen)
	<b>5f</b>	−11.93	Lys67 (NO <sub>2</sub> oxygen), Asp186 (oxime oxygen)
	NS-383	−11.39	Glu121 (oxime OH)

\* Units of Rosetta docking score. \*\* Ligand groups involved in the formation of hydrogen bonds are shown in parentheses.

We also performed molecular docking of compounds **5a**, **5d**, and **5f** into another important kinase, PIM1 (PDB: 2OBJ). The nitro group of **5d** had strong hydrogen bonding interactions with Lys67 and Asp186 of PIM1, which may be responsible for different orientation of the molecule compared to **5a**. Additionally, the oxime OH group of **5d** formed a hydrogen bond with Glu121 (Figure 4A, Table 5). On the other hand, molecule **5a** had quite a different orientation in the binding site and was H-bonded to Arg122, with participation of the oxime nitrogen atom (Figure 4B). Additionally, the compounds **5a** and **5d** overlapped significantly with the position of the co-crystallized pyridone ligand (6-(5-bromo-2-hydroxyphenyl)-2-oxo-4-phenyl-1,2-dihydropyridin-3-carbonitrile) present in the PDB 2OBJ structure [48]. It should be noted that the nitro-derivative **5d** had a more negative interface score than compound **5a**, in accordance with a higher binding affinity to PIM1. The inactive O-Ethyl oxime **5f** and low-activity compound NS-383 (based on binding affinity toward PIM1, see Table 4) were characterized by a lower interface score

(Table 5). These results, along with the data obtained for the docking of compound **5f** into DYRK1A (see above), highlight the importance of the unsubstituted oxime group =N-OH for effective binding to the investigated kinases.

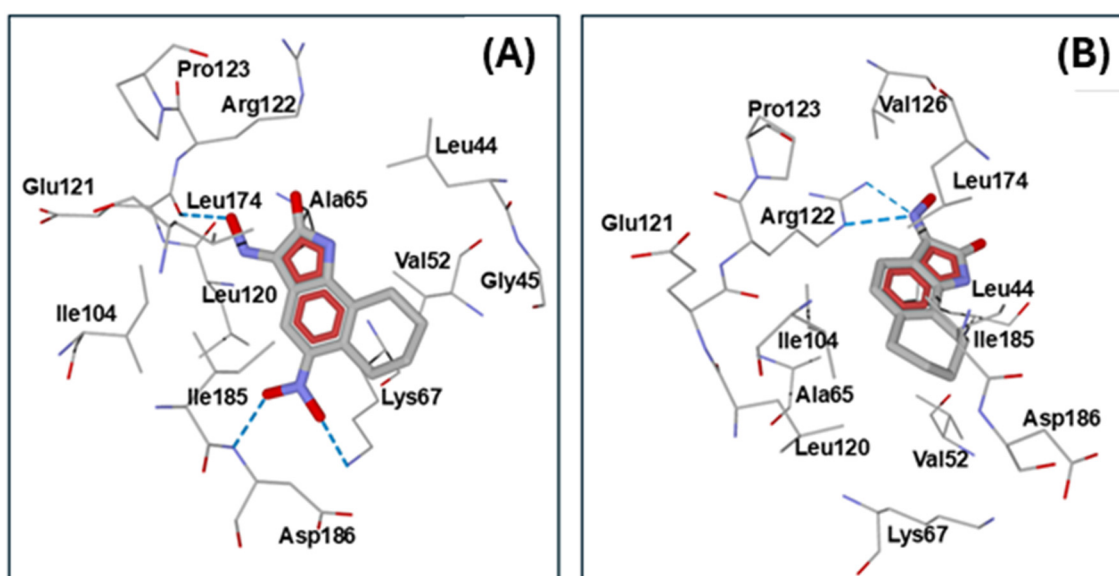


**Figure 4.** Docking poses of compounds **5d** (A) and **5a** (B) into the PIM1 binding site (PDB code 2OBJ). Residues within 4 Å from each pose are visible.

NS-102 (i.e., compound **5d** here) has been reported to be a glutamate receptor and NMDA receptor antagonist and has been used in several *in vivo* and *in vitro* models of neurodegenerative diseases [29–33]. Thus, the effects of NS-102 in such experiments and *in vivo* models should be reevaluated to consider the potential anti-inflammatory and neuroprotective effects via inhibition of kinases, including DYRK1A, PIM1, and Haspin.

It should be noted that indirubin oximes Ind14 and Ind15 (Figure 5) were reported to demonstrate high affinity for various kinases, including DYRK1A potential [25]. Of these, the carboxylic acid derivative Ind15 acts as an inhibitor of both DYRK1A and DYRK2 [49]. Structurally, Ind14 and Ind15 contain indoline moieties and an unsubstituted oxime group, similar to isatins **5a** and **5d**. However, compounds **5a–f** are based on a structurally distinct tricyclic scaffold compared to the indirubin derivatives.

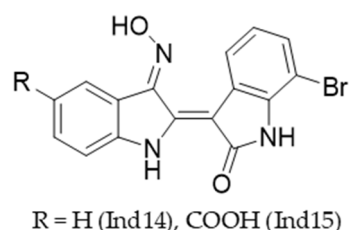


**Figure 5.** Chemical structures of indirubin oxime-based kinase inhibitors.

### 3. Materials and Methods

#### 3.1. Chemistry

##### 3.1.1. Compounds and Reagents

NS-383 (8-ethyl-6,7,8,9-tetrahydro-5-phenyl-1*H*-pyrrolo[3,2-*h*]isoquinolin-2,3-dione-3-oxime) was purchased from Tocris Bioscience (Ellisville, MD, EUA). All the other starting reagents were purchased from Sigma-Aldrich (Burlington, MA, USA).

### 3.1.2. Synthesis

Progress of the reactions was monitored by TLC on Sorbfil plates (sorbent—silica gel; base—aluminum; luminophore—254 nm). We determined the product melting points using a Stuart SMP30 instrument (Buch Holm, Herlev, Denmark). An Agilent Cary 630 FTIR (Agilent, Santa Clara, CA, USA) with an ATR attachment was used to obtain IR spectra. NMR spectra were recorded on a Bruker AM-400 spectrometer (Bruker, Billerica, MA, USA) with an operating frequency of 400 MHz ( $^1\text{H}$ ) and 100 MHz ( $^{13}\text{C}$ ). GC-MS analysis was performed on an Agilent 5975C instrument.

*6,7,8,9-Tetrahydro-1H-benzo[g]indol-2,3-dione (2)*: 18 mL of 75% sulfuric acid (30 g) was added to a 50 mL round bottom flask. The solution was cooled in an ice bath, and 1 g of 2-(hydroxyimino)-*N*-(5,6,7,8-tetrahydronaphthalen-1-yl)acetamide (4.6 mmol) was added in small portions, avoiding strong heating of the reaction mixture. After the tetrahydronaphthalene derivative was completely dissolved, the flask was placed in a water bath heated to 50 °C. The reaction continued for 20 min (TLC monitoring, hexane-ethyl acetate, 2:1). The mixture from the reaction flask was poured onto ice, and the formed precipitate was filtered. Yield 88%. Orange crystals, M.p. 235–238 °C, IR ( $\nu_{\text{max}}$ ,  $\text{cm}^{-1}$ ): 3439, 3188 (NH), 1730 (C=O), 1593, 1430 ( $\text{C}_{\text{Ar}}-\text{C}_{\text{Ar}}$ ), 1199, 1060, 967, 834, 675. NMR  $^1\text{H}$  (DMSO- $d_6$ ),  $\delta$ , ppm: 10.92 (s, 1H, NH), 7.19 (d,  $J$  7.8 Hz, 1H, ArH), 6.75 (d,  $J$  7.8 Hz, 1H, ArH), 2.71 (t,  $J$  6 Hz, 2H,  $\text{CH}_2$ ), 2.47 (t,  $J$  6 Hz, 2H,  $\text{CH}_2$ ), 1.78–1.66 (m, 4H,  $\text{CH}_2-\text{CH}_2$ ). NMR  $^{13}\text{C}$  (DMSO- $d_6$ ),  $\delta$ , ppm: 183.98, 160.58, 149.81, 149.29, 123.43, 121.43, 121.20, 115.00, 30.08, 23.07, 21.74, 21.56. GC/MS,  $m/z$ : 201.1 [ $\text{M}^+$ ].

*5-Nitro-6,7,8,9-tetrahydro-1H-benzo[g]indol-2,3-dione (3)*: 10 mL of 85% sulfuric acid (17.8 g) was cooled in an ice bath, 1 g of compound **2** was added in portions, avoiding strong heating of the reaction mixture. In parallel, a nitrating mixture was prepared from 7 mL of 85% sulfuric acid (12.5 g) and 1 g of concentrated nitric acid 65% (2 eq. with respect to the substrate). The nitrating mixture was cooled to 5 °C and added dropwise to the solution of isatin **2** in sulfuric acid, maintaining the temperature in the range of 5–20 °C. Upon completion of the reaction (after 1 h), the contents of the flask were poured onto ice, and the resulting light-yellow precipitate was filtered and dried. Product yield 97%. Orange crystals, M.p. 253–254 °C, IR ( $\nu_{\text{max}}$ ,  $\text{cm}^{-1}$ ): 3165 (NH), 1741 (C=O), 1614, 1593, 1525 (Ar- $\text{NO}_2$ ), 1430 ( $\text{C}_{\text{Ar}}-\text{C}_{\text{Ar}}$ ), 1355, 1302 (Ar- $\text{NO}_2$ ). NMR  $^1\text{H}$  (DMSO- $d_6$ ),  $\delta$ , ppm: 11.47 (s, 1H, NH), 7.86 (s, 1H, ArH), 2.91 (t,  $J$  6.5 Hz, 2H,  $\text{CH}_2$ ), 2.55 (t,  $J$  6 Hz, 2H,  $\text{CH}_2$ ), 1.81–1.65 (m, 4H,  $\text{CH}_2-\text{CH}_2$ ). NMR  $^{13}\text{C}$  (DMSO- $d_6$ ),  $\delta$ , ppm: 183.05, 161.02, 152.59, 145.03, 143.36, 123.34, 118.64, 114.95, 27.85, 24.13, 21.64, 20.75. LC/MS (ESI $^+$ );  $m/z$ : 269.0552 [ $\text{M} + \text{Na}$ ] $^+$  experimental ([ $\text{C}_{12}\text{H}_{10}\text{N}_2\text{O}_4 + \text{Na}$ ] $^+$  = 269.0538 theor.).

General procedure for the synthesis of oximes **5a–f**: In a 50 mL round bottom flask, 1 mmol of compound **2** or **3**, 1.2 mmol of a corresponding hydroxylamine hydrochloride, and 1.5 mmol of pyridine were dissolved into 20 mL of boiling ethanol. The reaction continued for 4 h. After complete conversion of the substrate (TLC monitoring), the reaction mass was poured into 100 mL of water, and the formed precipitate was filtered and dried. Product yields are given in Table 2.

*3-(Hydroxyimino)-1,3,6,7,8,9-hexahydro-2H-benzo[g]indol-2-one (5a)*: Yellow crystals, M.p. 250–252 °C, IR ( $\nu_{\text{max}}$ ,  $\text{cm}^{-1}$ ): 3165 (NH), 1693 (C=O), 1613 (C=N $_{\text{oxime}}$ ), 1577, 1420 ( $\text{C}_{\text{Ar}}-\text{C}_{\text{Ar}}$ ). NMR  $^1\text{H}$  (DMSO- $d_6$ ),  $\delta$ , ppm: 13.06 (s, 1H, OH), 10.53 (s, 1H, NH), 7.65 (d, 1H,  $J$  7.8 Hz, ArH), 6.72 (d, 1H,  $J$  7.8 Hz, ArH), 2.69 (t, 2H,  $J$  6 Hz,  $\text{CH}_2$ ), 2.53–2.45 (m, 2H,  $\text{CH}_2$ ), 1.78–1.63 (m, 4H,  $\text{CH}_2-\text{CH}_2$ ). NMR  $^{13}\text{C}$  (DMSO- $d_6$ ),  $\delta$ , ppm: 165.90, 145.02, 142.07, 141.51, 124.38, 122.96, 119.74, 113.48, 22.93, 23.98, 22.57, 22.35. LC/MS (ESI $^+$ );  $m/z$ : 217.0977 [ $\text{M} + \text{H}$ ] $^+$  experimental ([ $\text{C}_{12}\text{H}_{12}\text{N}_2\text{O}_2 + \text{H}$ ] $^+$  = 217.0977 theor.).

*3-(Methoxyimino)-1,3,6,7,8,9-hexahydro-2H-benzo[g]indol-2-one (5b)*: Yellow crystals, M.p. 237–239 °C, IR ( $\nu_{\text{max}}$ ,  $\text{cm}^{-1}$ ): 3155 (NH), 1715 (C=O), 1602 (C=N $_{\text{oxime}}$ ), 1586, 1430 ( $\text{C}_{\text{Ar}}-\text{C}_{\text{Ar}}$ ).

NMR  $^1\text{H}$  (DMSO- $d_6$ ),  $\delta$ , ppm: 10.65 (s, 1H, NH), 7.53 (d, 1H,  $J$  7.8 Hz, ArH), 6.71 (d, 1H,  $J$  7.8 Hz, ArH), 4.14 (s, 3H,  $\text{CH}_3$ ), 2.69 (t, 2H,  $J$  6 Hz,  $\text{CH}_2$ ), 2.53–2.47 (m, 2H,  $\text{CH}_2$ ), 1.77–1.65 (m, 4H,  $\text{CH}_2\text{-CH}_2$ ). NMR  $^{13}\text{C}$  (DMSO- $d_6$ ),  $\delta$ , ppm: 165.05, 144.74, 143.17, 142.22, 124.73, 123.11, 120.05, 113.10, 64.51, 29.99, 23.97, 22.47, 22.26. LC/MS (ESI $^+$ );  $m/z$ : 231.1135 [M + H] $^+$  experimental ([C $_{13}$ H $_{14}$ N $_2$ O $_2$  + H] $^+$  = 231.1134 theor.).

3-(Ethoxyimino)-1,3,6,7,8,9-hexahydro-2H-benzo[g]indol-2-one (5c): Yellow crystals, M.p. 242–244 °C, IR ( $\nu_{\text{max}}$ ,  $\text{cm}^{-1}$ ): 3155 (NH), 1715 (C=O), 1601 (C=N $_{\text{oxime}}$ ), 1430 (C $_{\text{Ar}}$ -C $_{\text{Ar}}$ ). NMR  $^1\text{H}$  (DMSO- $d_6$ ),  $\delta$ , ppm: 10.65 (s, 1H, NH), 7.54 (d, 1H,  $J$  7.8 Hz, ArH), 6.71 (d, 1H,  $J$  7.84 Hz, ArH), 4.39 (q, 2H,  $J$  7.08 Hz,  $\text{CH}_2\text{CH}_3$ ), 2.68 (t, 2H,  $J$  6 Hz,  $\text{CH}_2$ ), 2.53–2.46 (m, 2H,  $\text{CH}_2$ ), 1.76–1.65 (m, 4H,  $\text{CH}_2\text{-CH}_2$ ), 1.71 (t, 3H,  $J$  7 Hz,  $\text{CH}_3$ ). NMR  $^{13}\text{C}$  (DMSO- $d_6$ ),  $\delta$ , ppm: 165.18, 144.63, 143.00, 142.12, 124.64, 123.06, 119.97, 113.15, 72.28, 29.98, 23.97, 22.49, 22.27, 14.94. LC/MS (ESI $^+$ );  $m/z$ : 245.1295 [M + H] $^+$  experimental ([C $_{14}$ H $_{16}$ N $_2$ O $_2$  + H] $^+$  = 245.1290 theor.).

3-(Hydroxyimino)-5-nitro-1,3,6,7,8,9-hexahydro-2H-benzo[g]indol-2-one (5d): Yellow crystals, M.p. > 255 °C (decomp.), IR ( $\nu_{\text{max}}$ ,  $\text{cm}^{-1}$ ): 3275 (NH), 1721 (C=O), 1616 (C=N $_{\text{oxime}}$ ); 1504 (Ar-NO $_2$ ); 1456 (C $_{\text{Ar}}$ -C $_{\text{Ar}}$ ); 1300 (Ar-NO $_2$ ). NMR  $^1\text{H}$  (DMSO- $d_6$ ),  $\delta$ , ppm: 13.73 (s, 1H, OH), 11.20 (s, 1H, NH), 8.32 (s, 1H, ArH), 2.93 (t, 2H,  $J$  6 Hz,  $\text{CH}_2$ ), 2.60 (t, 2H,  $J$  6.5 Hz,  $\text{CH}_2$ ), 1.81–1.65 (m, 4H,  $\text{CH}_2\text{-CH}_2$ ). NMR  $^{13}\text{C}$  (DMSO- $d_6$ ),  $\delta$ , ppm: 165.71, 145.47, 144.20, 143.59, 138.23, 121.53, 121.16, 112.76, 27.68, 24.64, 21.93, 20.98. LC/MS (ESI $^+$ );  $m/z$ : 262.0827 [M + H] $^+$  experimental ([C $_{12}$ H $_{11}$ N $_3$ O $_4$  + H] $^+$  = 262.0828 theor.).

3-(Methoxyimino)-5-nitro-1,3,6,7,8,9-hexahydro-2H-benzo[g]indol-2-one (5e): Light-yellow crystals, M.p. > 264 °C (decomp.), IR ( $\nu_{\text{max}}$ ,  $\text{cm}^{-1}$ ): 3308 (NH), 1748 (C=O), 1609 (C=N $_{\text{oxime}}$ ), 1504 (Ar-NO $_2$ ), 1450 (C $_{\text{Ar}}$ -C $_{\text{Ar}}$ ), 1297 (Ar-NO $_2$ ). NMR  $^1\text{H}$  (DMSO- $d_6$ ),  $\delta$ , ppm: 11.26 (s, 1H, NH), 8.16 (s, 1H, ArH), 4.23 (s, 3H,  $\text{CH}_3$ ), 2.9 (t, 2H,  $J$  6 Hz,  $\text{CH}_2$ ), 2.56 (t, 2H,  $J$  6.5 Hz,  $\text{CH}_2$ ), 1.78–1.67 (m, 4H,  $\text{CH}_2\text{-CH}_2$ ). NMR  $^{13}\text{C}$  (DMSO- $d_6$ ),  $\delta$ , ppm: 166.50, 146.02, 143.88, 143.00, 140.13, 122.56, 120.15, 112.99, 60.32, 28.10, 24.55, 21.61, 20.06. LC/MS (ESI $^+$ );  $m/z$ : 276.0989 [M + H] $^+$  experimental ([C $_{13}$ H $_{13}$ N $_3$ O $_4$  + H] $^+$  = 276.0984 theor.).

3-(Ethoxyimino)-5-nitro-1,3,6,7,8,9-hexahydro-2H-benzo[g]indol-2-one (5f): Light-yellow crystals, M.p. > 268 °C (decomp.), IR ( $\nu_{\text{max}}$ ,  $\text{cm}^{-1}$ ): 3268 (NH), 1732 (C=O), 1603 (C=N $_{\text{oxime}}$ ), 1520 (Ar-NO $_2$ ), 1420 (C $_{\text{Ar}}$ -C $_{\text{Ar}}$ ), 1383, 1323 (Ar-NO $_2$ ). NMR  $^1\text{H}$  (DMSO- $d_6$ ),  $\delta$ , ppm: 11.26 (s, 1H, NH), 8.18 (s, 1H, ArH), 4.48 (q, 2H,  $J$  7 Hz,  $\text{CH}_2\text{CH}_3$ ), 2.9 (t, 2H,  $J$  6 Hz,  $\text{CH}_2$ ), 2.57 (t, 2H,  $J$  6 Hz,  $\text{CH}_2$ ), 1.78–1.65 (m, 4H,  $\text{CH}_2\text{-CH}_2$ ), 1.37 (t, 3H,  $J$  7 Hz,  $\text{CH}_3$ ). NMR  $^{13}\text{C}$  (DMSO- $d_6$ ),  $\delta$ , ppm: 167.70, 146.34, 144.16, 143.12, 139.81, 122.83, 120.01, 113.15, 74.70, 28.12, 24.63, 21.83, 19.99, 14.92. LC/MS (ESI $^+$ );  $m/z$ : 290.1151 [M + H] $^+$  experimental ([C $_{14}$ H $_{15}$ N $_3$ O $_4$  + H] $^+$  = 290.1141 theor.).

### 3.2. Biological Assays

#### 3.2.1. Cell Culture

Human THP-1Blue monocytic cells stably transfected with a secreted embryonic alkaline phosphatase gene that is under control of a NF- $\kappa$ B/AP-1-inducible promoter were obtained from InvivoGen (San Diego, CA, USA). These cells were cultured in RPMI 1640 medium (Mediatech Inc., Herndon, VA, USA) containing 10% ( $v/v$ ) fetal bovine serum (FBS), 100  $\mu\text{g}/\text{mL}$  streptomycin, 100 U/mL penicillin, 100  $\mu\text{g}/\text{mL}$  phleomycin (Zeocin), and 10  $\mu\text{g}/\text{mL}$  blasticidin S (all from Sigma-Aldrich, St. Louis, MO, USA).

Human MonoMac-6 monocyte/macrophage cells (Deutsche Sammlung von Mikroorganismen und Zellkulturen GmbH, Braunschweig, Germany) were cultured in RPMI 1640 medium containing 10% ( $v/v$ ) FBS, 10  $\mu\text{g}/\text{mL}$  bovine insulin, 100  $\mu\text{g}/\text{mL}$  streptomycin, and 100 U/mL penicillin.

### 3.2.2. Evaluation of AP-1/NF- $\kappa$ B Activation

After incubation of THP-1Blue cells ( $2 \times 10^5$  cells/well) with test compounds or control DMSO (1% final concentration) for 30 min, 250 ng/mL of lipopolysaccharide (LPS; from *Escherichia coli* strain 0111:B4) was added, and the cells were incubated for 24 h. Secreted alkaline phosphatase activity was assessed in the cell supernatants using the QUANTI-Blue mix (InvivoGen; absorbance at 655 nm) and compared with positive controls treated with LPS alone. Compound concentrations that inhibited 50% of the NF- $\kappa$ B reporter activity (IC<sub>50</sub>) were determined.

### 3.2.3. Analysis of Cytokine Production

An IL-6 ELISA kit (BD Biosciences, San Jose, CA, USA) was used to assess the effect of selected compounds on IL-6 production. MonoMac-6 cells were plated in 96-well plates at a density of  $2 \times 10^5$  cells/well in culture medium supplemented with 3% (*v/v*) endotoxin-free FBS. Cells were pretreated with test compound or DMSO for 30 min, followed by addition of 200 ng/mL LPS for 24 h. For selected compounds, the IC<sub>50</sub> for cytokine production was calculated by plotting percentage inhibition against the logarithm of inhibitor concentration (at least five points).

A multiplex human cytokine ELISA kit from Anogen (Mississauga, ON, Canada) was used to evaluate various cytokines (IL-1 $\alpha$ , IL-1 $\beta$ , IL-6, GM-CSF, MCP-1, IFN- $\gamma$ , and TNF) in the supernatants of MonoMac-6 cells.

### 3.2.4. Cytotoxicity Assay

Cytotoxicity was analyzed with a CellTiter-Glo Luminescent Cell Viability Assay Kit from Promega (Madison, WI, USA) according to the manufacturer's protocol. THP-1Blue cells were treated with varying concentrations of the test compounds (up to 50  $\mu$ M) and cultivated for 24 h. After treatment, the cells were allowed to equilibrate to room temperature for 30 min, the substrate was added, and the samples were analyzed with a Fluoroscan Ascent FL (Thermo Fisher Scientific, Waltham, MA, USA).

### 3.2.5. Kinase Profiling and K<sub>d</sub> Determination

Kinase profiling was performed by KINOMEScan (Eurofins Pharma Discovery, San Diego, CA, USA), using a panel of 423 protein kinases, as described previously [43]. Compounds were submitted for dissociation constant (K<sub>d</sub>) determination toward several target kinases using KINOMEScan. In brief, kinases were produced and displayed on T7 phages or expressed in HEK-293 cells. Binding reactions were performed at room temperature for 1 h, and the fraction of kinase not bound to the test compound was determined by capture with an immobilized affinity ligand and quantified by quantitative polymerase chain reaction. The primary screening at fixed concentrations of the compound was performed in duplicate. For dissociation constant K<sub>d</sub> determination, a 12-point half-log dilution series (a maximum concentration of 33  $\mu$ M) was used. Assays were performed in duplicate, and their average mean values are displayed.

## 3.3. Molecular Docking

The 3D structures of ligands **5a** and **5d** were built using ChemOffice 2016 software, pre-optimized with the MM2 force field, and saved in the SDF format. The DYRK1A and PIM1 structures were downloaded from PDB (3ANQ [46] and 2OBJ [48] entries, respectively). These protein structures, along with prepared molecular models of the investigated isatin derivatives, were uploaded to the ROSIE web server [50], where the ligand docking protocol [51,52] was applied. The search areas for docking were positioned at the geometric centers of gravity of the (1Z)-1-(3-ethyl-5-hydroxy-1,3-benzothiazol-2(3H)-ylidene)propan-

2-one and 6-(5-bromo-2-hydroxyphenyl)-2-oxo-4-phenyl-1,2-dihydropyridin-3-carbonitrile ligands co-crystallized in 3ANQ and 2OBJ structures, respectively. Up to 200 conformers were generated for each ligand with the use of the BCL conformer generation algorithm [53] incorporated in the ROSIE ligand docking protocol. For each of the compounds, 2000 docking runs were performed. The obtained docking poses with the most negative docking scores were saved and analyzed using the Molegro Virtual Docker 6.0 (MVD) program (CLC Bio, Copenhagen, Denmark).

#### 4. Conclusions

Synthetic methods were developed to obtain tricyclic isatin analogue **2**, its nitro-derivative **3**, and the corresponding oximes **5a** and **5d**. These synthetic methods ensured high yields of the products along with good purity. The *O*-alkyl oximes **5b**, **5c**, **5e**, and **5f** were synthesized here for the first time and characterized. Evaluation of their biological activity showed that compounds **5a** and **5d** (a.k.a. NS-102) had potent anti-inflammatory activity and inhibited LPS-induced NF- $\kappa$ B/AP-1 transcriptional activity and proinflammatory cytokine/chemokine production by monocyte/macrophage cells. Analysis of their kinase targets showed that these compounds exhibited nanomolar/submicromolar binding affinity toward several kinase targets, including DYRK1A, DYRK1B, PIM1, Haspin, HIPK1-3, IRAK1, NEK10, and DAPK1-3. Furthermore, molecular modeling suggested modes of binding interaction of selected compounds in the DYRK1A and PIM1 catalytic sites that agreed with the experimental binding data. Thus, these tricyclic isatin oximes may have the potential to be developed into anti-inflammatory drugs, possibly for the treatment of neurodegenerative diseases.

**Supplementary Materials:** The following supporting information can be downloaded at: <https://www.mdpi.com/article/10.3390/molecules30142914/s1>, Table S1. Optimization of the reaction conditions on the synthesis of 6,7,8,9-tetrahydro-1*H*-benzo[*g*]indol-2,3-dione (compound **2**) from 2-(hydroxyimino)-*N*-(5,6,7,8-tetrahydronaphthalen-1-yl)-acetamide (compound **1**). Table S2. Kinase profile of NS-102 (compound **5d**). The kinases were evaluated using the KINOMEScan platform, as described under Materials and Methods. Shown is the percentage inhibition of binding to an active-site directed ligand for each of the indicated kinases after treatment with 10  $\mu$ M NS-102.

**Author Contributions:** Conceptualization, I.A.S. and A.I.K.; data curation, A.I.K. and M.T.Q.; methodology, A.V.U., I.A.S. and A.I.K.; formal analysis, A.V.U., I.A.S. and A.I.K.; chemical synthesis and physical characterization, A.V.U. and A.I.K.; molecular modeling, A.I.K.; writing—original draft preparation, A.V.U., I.A.S. and A.I.K.; writing—review and editing, I.A.S., M.T.Q. and A.I.K.; supervision, A.I.K. and M.T.Q. All authors have read and agreed to the published version of the manuscript.

**Funding:** The synthesis of the isatin derivatives and the molecular modeling study were funded by the Russian Science Foundation (project No. 24-15-00334); the biological studies were supported by the National Institutes of Health IDeA Program Grant GM103474 and the Montana State University Agricultural Experiment Station.

**Institutional Review Board Statement:** Not applicable.

**Informed Consent Statement:** Not applicable.

**Data Availability Statement:** Data is contained within the article and Supplementary Materials.

**Conflicts of Interest:** The authors declare no conflicts of interest.

## References

1. Frost, D.; Meechoovet, B.; Wang, T.; Gately, S.; Giorgetti, M.; Shcherbakova, I.; Dunckley, T. Carboline Compounds, Including Harmine, Inhibit DYRK1A and Tau Phosphorylation at Multiple Alzheimer's Disease-Related Sites. *PLoS ONE* **2011**, *6*, e19264. [[CrossRef](#)] [[PubMed](#)]
2. Latosińska, M.; Latosińska, J.N. Serine/Threonine Protein Kinases as Attractive Targets for Anti-Cancer Drugs—An Innovative Approach to Ligand Tuning Using Combined Quantum Chemical Calculations, Molecular Docking, Molecular Dynamic Simulations, and Network-like Similarity Graphs. *Molecules* **2024**, *29*, 3199. [[CrossRef](#)] [[PubMed](#)]
3. Narlik-Grassow, M.; Blanco-Aparicio, C.; Carnero, A. The PIM family of serine/threonine kinases in cancer. *Med. Res. Rev.* **2013**, *34*, 136–159. [[CrossRef](#)]
4. Quadri, R.; Sertic, S.; Muzi-Falconi, M. Roles and regulation of Haspin kinase and its impact on carcinogenesis. *Cell. Signal.* **2022**, *93*, 110303. [[CrossRef](#)] [[PubMed](#)]
5. Nishida-Fukuda, H.; Tokuhiko, K.; Ando, Y.; Matsushita, H.; Wada, M.; Tanaka, H. Evaluation of the antiproliferative effects of the HASPIN inhibitor CHR-6494 in breast cancer cell lines. *PLoS ONE* **2021**, *16*, e0249912. [[CrossRef](#)]
6. Lin, C.-I.; Chen, Z.-C.; Chen, C.-H.; Chang, Y.-H.; Lee, T.-C.; Tang, T.-T.; Yang, C.-M.; Tsai, M.-C.; Huang, C.-C.; Yang, T.-W.; et al. Co-inhibition of Aurora A and Haspin kinases enhances survivin blockage and p53 induction for mitotic catastrophe and apoptosis in human colorectal cancer. *Biochem. Pharmacol.* **2022**, *206*, 115289. [[CrossRef](#)]
7. Ananthapadmanabhan, V.; Shows, K.H.; Dickinson, A.J.; Litovchick, L. Insights from the protein interaction Universe of the multifunctional Goldilocks kinase DYRK1A. *Front. Cell Dev. Biol.* **2023**, *11*, 1277537. [[CrossRef](#)]
8. Kimura, R.; Kamino, K.; Yamamoto, M.; Nuripa, A.; Kida, T.; Kazui, H.; Hashimoto, R.; Tanaka, T.; Kudo, T.; Yamagata, H.; et al. The DYRK1A gene, encoded in chromosome 21 Down syndrome critical region, bridges between-amyloid production and tau phosphorylation in Alzheimer disease. *Hum. Mol. Genet.* **2006**, *16*, 15–23. [[CrossRef](#)]
9. Wegiel, J.; Dowjat, K.; Kaczmarek, W.; Kuchna, I.; Nowicki, K.; Frackowiak, J.; Kolecka, B.M.; Wegiel, J.; Silverman, W.P.; Reisberg, B.; et al. The role of overexpressed DYRK1A protein in the early onset of neurofibrillary degeneration in Down syndrome. *Acta Neuropathol.* **2008**, *116*, 391–407. [[CrossRef](#)]
10. Meur, S.; Mukherjee, S.; Roy, S.; Karati, D. Role of PIM Kinase Inhibitor in the Treatment of Alzheimers Disease. *Mol. Neurobiol.* **2024**, *61*, 10941–10955. [[CrossRef](#)]
11. Tanaka, H.; Matsushita, H.; Tokuhiko, K.; Fukunari, A.; Ando, Y. Ingestion of soybean sprouts containing a HASPIN inhibitor improves condition in a mouse model of Alzheimer's disease. *Biology* **2023**, *12*, 320. [[CrossRef](#)]
12. Acitelli, E.; Maiorca, C.; Grani, G.; Maranghi, M. Metabolic adverse events of multitarget kinase inhibitors: A systematic review. *Endocrine* **2023**, *81*, 16–29. [[CrossRef](#)]
13. Chen, S.; Yang, Y.; Yuan, Y.; Liu, B. Targeting PIM kinases in cancer therapy: An update on pharmacological small-molecule inhibitors. *Eur. J. Med. Chem.* **2023**, *264*, 116016. [[CrossRef](#)] [[PubMed](#)]
14. Baek, H.S.; Kim, N.; Park, J.W.; Kwon, T.K.; Kim, S. The role of Pim-1 kinases in inflammatory signaling pathways. *Inflamm. Res.* **2024**, *73*, 1671–1685. [[CrossRef](#)] [[PubMed](#)]
15. Yang, Y.; Fan, X.; Liu, Y.; Ye, D.; Liu, C.; Yang, H.; Su, Z.; Zhang, Y.; Liu, Y. Function and inhibition of DYRK1A: Emerging roles of treating multiple human diseases. *Biochem. Pharmacol.* **2023**, *212*, 115521. [[CrossRef](#)]
16. García, E.G.; Varas, P.; González-Naranjo, P.; Ulzurrun, E.; Marcos-Ayuso, G.; Pérez, C.; Páez, J.A.; Insua, D.R.; Santana, S.R.; Campillo, N.E. AI-driven de novo design and development of nontoxic DYRK1A inhibitors. *J. Med. Chem.* **2025**, *68*, 10346–10364. [[CrossRef](#)]
17. Kestav, K.; Uri, A.; Lavogina, D. Structure, roles and inhibitors of a mitotic protein kinase Haspin. *Curr. Med. Chem.* **2017**, *24*, 2276–2293. [[CrossRef](#)]
18. Corsello, S.M.; Bittker, J.A.; Liu, Z.; Gould, J.; McCarren, P.; Hirschman, J.E.; Johnston, S.E.; Vrcic, A.; Wong, B.; Khan, M.; et al. The Drug Repurposing Hub: A next-generation drug library and information resource. *Nat. Med.* **2017**, *23*, 405–408. [[CrossRef](#)]
19. Campillos, M.; Kuhn, M.; Gavin, A.-C.; Jensen, L.J.; Bork, P. Drug target identification using side-effect similarity. *Science* **2008**, *321*, 263–266. [[CrossRef](#)]
20. Schepetkin, I.A.; Karpenko, O.S.; Kovrizhina, A.R.; Kirpotina, L.N.; Khlebnikov, A.I.; Chekal, S.I.; Radudik, A.V.; Shybinska, M.O.; Quinn, M.T. Novel tryptanthrin derivatives with selectivity as c-Jun N-terminal kinase (JNK) 3 inhibitors. *Molecules* **2023**, *28*, 4806. [[CrossRef](#)]
21. Schepetkin, I.A.; Kovrizhina, A.R.; Stankevich, K.S.; Khlebnikov, A.I.; Kirpotina, L.N.; Quinn, M.T.; Cook, M.J. Design, synthesis and biological evaluation of novel O-substituted tryptanthrin oxime derivatives as c-Jun N-terminal kinase inhibitors. *Front. Pharmacol.* **2022**, *13*, 958687. [[CrossRef](#)] [[PubMed](#)]
22. Schepetkin, I.A.; Khlebnikov, A.I.; Potapov, A.S.; Kovrizhina, A.R.; Matveevskaya, V.V.; Belyanin, M.L.; Atochin, D.N.; Zanoza, S.O.; Gaidarzhly, N.M.; Lyakhov, S.A.; et al. Synthesis, biological evaluation, and molecular modeling of 11H-indeno-1, 2b-quinoxalin-11-one derivatives and tryptanthrin-6-oxime as c-Jun N-terminal kinase inhibitors. *Eur. J. Med. Chem.* **2019**, *161*, 179–191. [[CrossRef](#)]

23. Nie, Z.; Xia, X.; Zhao, Y.; Zhang, S.; Zhang, Y.; Wang, J. JNK selective inhibitor, IQ-1S, protects the mice against lipopolysaccharides-induced sepsis. *Bioorganic Med. Chem.* **2021**, *30*, 115945. [[CrossRef](#)] [[PubMed](#)]
24. Beauchard, A.; Laborie, H.; Rouillard, H.; Lozach, O.; Ferandin, Y.; Guével, R.L.; Guguen-Guillouzo, C.; Meijer, L.; Besson, T.; Thiéry, V. Synthesis and kinase inhibitory activity of novel substituted indigoids. *Bioorganic Med. Chem.* **2009**, *17*, 6257–6263. [[CrossRef](#)] [[PubMed](#)]
25. Schepetkin, I.A.; Plotnikov, M.B.; Khlebnikov, A.I.; Plotnikova, T.M.; Quinn, M.T. Oximes: Novel Therapeutics with Anticancer and Anti-Inflammatory Potential. *Biomolecules* **2021**, *11*, 777. [[CrossRef](#)]
26. Ishikura, M.; Abe, T.; Choshi, T.; Hibino, S. Simple indole alkaloids and those with a non-rearranged monoterpenoid unit. *Nat. Prod. Rep.* **2013**, *30*, 694–752. [[CrossRef](#)]
27. Capó, T.; Rebassa, J.B.; Raïch, I.; Lillo, J.; Badia, P.; Navarro, G.; Reyes-Resina, I. Future perspectives of NMDAR in CNS disorders. *Molecules* **2025**, *30*, 877. [[CrossRef](#)]
28. Tripathi, S.; Sharma, Y.; Kumar, D. Exploring New Structures of Kinase Inhibitors and Multitarget Strategies in Alzheimer's Disease Treatment. *Protein Pept. Lett.* **2025**, *32*, 2–17. [[CrossRef](#)]
29. Jakobsen, B.; Tasker, A.; Zimmer, J. Domoic acid neurotoxicity in hippocampal slice cultures. *Amino Acids* **2002**, *23*, 37–44. [[CrossRef](#)]
30. Tasker, R.A.; Strain, S.M.; Drejer, J. Selective reduction in domoic acid toxicity in vivo by a novel non-N-methyl-D-aspartate receptor antagonist. *Can. J. Physiol. Pharmacol.* **1996**, *74*, 1047–1054. [[CrossRef](#)]
31. Li, Q.; Ma, T.-L.; Qiu, Y.-Q.; Cui, W.-Q.; Chen, T.; Zhang, W.-W.; Wang, J.; Mao-Ying, Q.-L.; Mi, W.-L.; Wang, Y.-Q.; et al. Connexin 36 mediates orofacial pain hypersensitivity through GluK2 and TRPA1. *Neurosci. Bull.* **2020**, *36*, 1484–1499. [[CrossRef](#)] [[PubMed](#)]
32. Perkinson, M.S.; Sihra, T.S. A high-affinity presynaptic kainate-type glutamate receptor facilitates glutamate exocytosis from cerebral cortex nerve terminals (synaptosomes). *Neuroscience* **1999**, *90*, 1281–1292. [[CrossRef](#)]
33. Kamiya, H.; Ozawa, S. Kainate receptor-mediated inhibition of presynaptic Ca<sup>2+</sup> influx and EPSP in area CA1 of the rat hippocampus. *J. Physiol.* **1998**, *509*, 833–845. [[CrossRef](#)] [[PubMed](#)]
34. Munro, G.; Christensen, J.K.; Erichsen, H.K.; Dyhring, T.; Demnitz, J.; Dam, E.; Ahring, P.K. NS383 Selectively Inhibits Acid-Sensing Ion Channels Containing 1a and 3 Subunits to Reverse Inflammatory and Neuropathic Hyperalgesia in Rats. *Cns Neurosci. Ther.* **2015**, *22*, 135–145. [[CrossRef](#)]
35. Sun, A.W.; Wu, M.H.; Vijayalingam, M.; Wacker, M.J.; Chu, X.-P. The role of zinc in modulating acid-sensing ion channel function. *Biomolecules* **2023**, *13*, 229. [[CrossRef](#)] [[PubMed](#)]
36. Wätjen, F.; Nielsen, E.; Drejer, J.; Jensen, L.H. Isatin oximes-A novel series of bioavailable non-NMDA antagonists. *Bioorganic Med. Chem. Lett.* **1993**, *3*, 105–106. [[CrossRef](#)]
37. Al-Khuzai, M.G.A.; Fahad, M.M.; Al-Safi, A.J. Synthesis, reaction and biological importance of isatin derivatives. *Biomed. Chem. Sci.* **2022**, *1*, 193–206. [[CrossRef](#)]
38. Zhungietu, G.I.; Rechter, M.A. *Isatin and Its Derivatives*; Academy of Sciences of the Moldavian SSR, Institute of Chemistry: Chisinau, Moldova, 1977. (In Russian)
39. Popp, F.D.; McEwen, W.E. Polyphosphoric acids as a reagent in organic chemistry. *Chem. Rev.* **1958**, *58*, 321–401. [[CrossRef](#)]
40. Baker, B.R.; Schaub, R.E.; Joseph, J.P.; McEvoy, F.J.; Williams, J.H. An antimalarial alkaloid from hydrangea. XV. Synthesis of 5-, 6-, 7-, and 8-derivatives with two identical substituents. *J. Org. Chem.* **1952**, *17*, 149–156. [[CrossRef](#)]
41. Mazhilis, L.I.; Terent'Ev, P.B.; Bolotin, V.A. Mononitration of derivatives of benzisatins. *Chem. Heterocycl. Compd.* **1989**, *25*, 50–55. [[CrossRef](#)]
42. Adcock, I.M.; Caramori, G. Cross-talk between pro-inflammatory transcription factors and glucocorticoids. *Immunol. Cell Biol.* **2001**, *79*, 376–384. [[CrossRef](#)] [[PubMed](#)]
43. Karaman, M.W.; Herrgard, S.; Treiber, D.K.; Gallant, P.; Atteridge, C.E.; Campbell, B.T.; Chan, K.W.; Ciceri, P.; Davis, M.I.; Edeen, P.T.; et al. A quantitative analysis of kinase inhibitor selectivity. *Nat. Biotechnol.* **2008**, *26*, 127–132. [[CrossRef](#)] [[PubMed](#)]
44. Fabian, M.A.; Biggs, W.H.; Treiber, D.K.; Atteridge, C.E.; Azimioara, M.D.; Benedetti, M.G.; Carter, T.A.; Ciceri, P.; Edeen, P.T.; Floyd, M.; et al. A small molecule-kinase interaction map for clinical kinase inhibitors. *Nat. Biotechnol.* **2005**, *23*, 329–336. [[CrossRef](#)] [[PubMed](#)]
45. Hoang, V.T.; Nyswaner, K.; Torres-Ayuso, P.; Brognard, J. The protein kinase MAP3K19 phosphorylates MAP2Ks and thereby activates ERK and JNK kinases and increases viability of KRAS-mutant lung cancer cells. *J. Biol. Chem.* **2020**, *295*, 8470–8479. [[CrossRef](#)]
46. Ogawa, Y.; Nonaka, Y.; Goto, T.; Ohnishi, E.; Hiramatsu, T.; Kii, I.; Yoshida, M.; Ikura, T.; Onogi, H.; Shibuya, H.; et al. Development of a novel selective inhibitor of the Down syndrome-related kinase DYRK1A. *Nat. Commun.* **2010**, *1*, 86. [[CrossRef](#)] [[PubMed](#)]
47. Masaki, S.; Kii, I.; Sumida, Y.; Kato-Sumida, T.; Ogawa, Y.; Ito, N.; Nakamura, M.; Sonamoto, R.; Kataoka, N.; Hosoya, T.; et al. Design and synthesis of a potent inhibitor of class 1 DYRK kinases as a suppressor of adipogenesis. *Bioorganic Med. Chem.* **2015**, *23*, 4434–4441. [[CrossRef](#)]

48. Cheney, I.W.; Yan, S.; Appleby, T.; Walker, H.; Vo, T.; Yao, N.; Hamatake, R.; Hong, Z.; Wu, J.Z. Identification and structure-activity relationships of substituted pyridones as inhibitors of Pim-1 kinase. *Bioorganic Med. Chem. Lett.* **2007**, *17*, 1679–1683. [[CrossRef](#)]
49. Myriantopoulos, V.; Kritsanida, M.; Gaboriaud-Kolar, N.; Magiatis, P.; Ferandin, Y.; Durieu, E.; Lozach, O.; Cappel, D.; Soundararajan, M.; Filippakopoulos, P.; et al. Novel inverse binding mode of indirubin derivatives yields improved selectivity for DYRK kinases. *ACS Med. Chem. Lett.* **2013**, *4*, 22–26. [[CrossRef](#)] [[PubMed](#)]
50. Lyskov, S.; Chou, F.-C.; Conchúir, S.; Der, B.S.; Drew, K.; Kuroda, D.; Xu, J.; Weitzner, B.D.; Renfrew, P.D.; Sripakdeevong, P.; et al. Serverification of molecular modeling applications: The Rosetta Online Server that Includes Everyone (ROSIE). *PLoS ONE* **2013**, *8*, e63906. [[CrossRef](#)]
51. DeLuca, S.; Khar, K.; Meiler, J. Fully flexible docking of medium sized ligand libraries with Rosetta ligand. *PLoS ONE* **2015**, *10*, e0132508. [[CrossRef](#)]
52. Combs, S.A.; DeLuca, S.L.; DeLuca, S.H.; Lemmon, G.H.; Nannemann, D.P.; Nguyen, E.D.; Willis, J.R.; Sheehan, J.H.; Meiler, J. Small-molecule ligand docking into comparative models with Rosetta. *Nat. Protoc.* **2013**, *8*, 1277–1298. [[CrossRef](#)] [[PubMed](#)]
53. Kothiwale, S.; Mendenhall, J.L.; Meiler, J. BCL::CONF: Small molecule conformational sampling using a knowledge based rotamer library. *J. Cheminform.* **2015**, *7*, 47. [[CrossRef](#)] [[PubMed](#)]

**Disclaimer/Publisher’s Note:** The statements, opinions and data contained in all publications are solely those of the individual author(s) and contributor(s) and not of MDPI and/or the editor(s). MDPI and/or the editor(s) disclaim responsibility for any injury to people or property resulting from any ideas, methods, instructions or products referred to in the content.